Partition function zeros of the square-lattice Ising model with nearest- and next-nearest-neighbor interactions

Seung-Yeon Kim*
School of Liberal Arts and Sciences, Chungju National University, Chungju 380-702, Korea
(Received 2 December 2009; published 22 March 2010)

The distributions of the partition function zeros in the complex $a=e^{2\beta J_1}$ plane of the square-lattice Ising model with nearest-neighbor (J_1) and next-nearest-neighbor (J_2) interactions are investigated as a function of $R=J_2/J_1$. Starting from the well-known two-circle distribution of the zeros $a=\pm 1+\sqrt{2}e^{i\theta}$ for $R=0$, finally the partition function zeros lie on the unit circle $a=e^{i\theta}$ for $R=\infty$. Between these two ends, the changes in the zero distributions are described. Using the partition function zeros, the critical point $a_c(R)$ and the thermal scaling exponent $y_t(R)$ are estimated for the Ising ferromagnet (equivalently, antiferromagnet) and superantiferromagnet. For the special case of $R=\frac{1}{2}$, the possible implications of the zero distributions are also discussed.

DOI: 10.1103/PhysRevE.81.031120 PACS number(s): 05.50.+q, 05.70.−a, 64.60.Cn, 75.10.Hk

I. INTRODUCTION

The square-lattice Ising model with nearest-neighbor (J_1) and next-nearest-neighbor (J_2) interactions has four different phases—paramagnetic, ferromagnetic, antiferromagnetic, and superantiferromagnetic phases. The superantiferromagnetic ground states correspond to the alternate arrangements of ferromagnetic rows or columns with oppositely oriented up and down spins. The square-lattice Ising model is exactly solvable only in the special cases of $J_1=0$ or $J_2=0$. Until now, various methods have been applied to understand the phase diagram of the model and/or to determine its critical exponents [1–18]. However, even the critical temperatures have not been known exactly although there have been two closed-form approximations for the critical temperatures, Zandvliet formula for the paramagnetic-ferromagnetic (or paramagnetic-antiferromagnetic) transition temperatures [14] and Berker-Hui formula for the paramagnetic-superantiferromagnetic transition temperatures [11].

Yang and Lee proposed the important concept of the partition function zeros in the complex fugacity plane, and found the famous circle theorem that all the zeros of the nearest-neighbor Ising ferromagnet lie on the unit circle in the complex fugacity plane [19]. Also, Fisher introduced the partition function zeros in the complex temperature plane of the square-lattice Ising model for $J_2=0$ [20]. Because the properties of the partition function zeros of a given system provided the valuable information on its exact solution, the earlier studies on partition function zeros were mainly performed in the fields of mathematical physics and rigorous statistical mechanics. Nowadays, the concept of partition function zeros is applied to all fields of physics, and they are popularly used as one of the most effective methods to determine the critical temperatures and exponents [21–24].

Recently, Monroe and Kim [15] have applied the method of partition function zeros to the square-lattice Ising model with both J_1 and J_2 interactions for the first time. They have shown that the partition function zeros of the model can be used to obtain the accurate estimates of not only the phase transition points in the phase diagram but also the values for the correlation-length critical exponent ν. In particular, they have clearly shown the nonuniversal critical behavior of the square-lattice Ising superantiferromagnet for $J_2/J_1=1$ and 2. In this paper, we try to complete the earlier work of Monroe and Kim, and we investigate the veiled properties of the partition function zeros for the square-lattice Ising model with both J_1 and J_2 interactions that have not been understood in the paper of Monroe and Kim. Also, we study the critical behaviors of the square-lattice Ising ferromagnet (equivalently, antiferromagnet) and superantiferromagnet using the partition function zeros for more extensive values of J_2/J_1.

II. DENSITY OF STATES

The Ising model with nearest-neighbor (J_1) and next-nearest-neighbor (J_2) interactions is defined by

$$\mathcal{H}=-J_1\sum_{\langle i,j\rangle}(\sigma_i\sigma_j+1)-J_2\sum_{(i,k)}(\sigma_i\sigma_k+1), \tag{1}$$

where $\sigma_i=\pm 1$ and the sums are over all nearest-neighbor $\langle i,j\rangle$ and next-nearest-neighbor (i,k) pairs, respectively. If we define the density of states, $\Omega(E_1,E_2)$, with the given energies $E_1=\frac{1}{2}\Sigma_{\langle i,j\rangle}(\sigma_i\sigma_j+1)$ and $E_2=\frac{1}{2}\Sigma_{(i,k)}(\sigma_i\sigma_k+1)$, the partition function of the model is written as

$$Z=\sum_{E_1=0}^{N_1}\sum_{E_2=0}^{N_2}\Omega(E_1,E_2)e^{2\beta(J_1E_1+J_2E_2)}, \tag{2}$$

where N_1 and N_2 are the numbers of nearest- and next-nearest-neighbor bonds, respectively.

The *exact* integer values for the density of states $\Omega(E_1,E_2)$ are obtained with the modified version (see Appendix) of the microcanonical transfer matrix for $J_2=0$ [23] on $L\times 2L$ (up to $L=9$) square lattices with free boundary conditions in the L-direction and periodic boundary conditions in the $2L$-direction ($N_1=4L^2-2L$ and $N_2=4L^2-4L$). These boundary conditions are very effective in studying the square-lattice Ising model with next-nearest-neighbor interactions [15]. For $L=9$, the CPU time for the evaluation of

*sykimm@cjnu.ac.kr

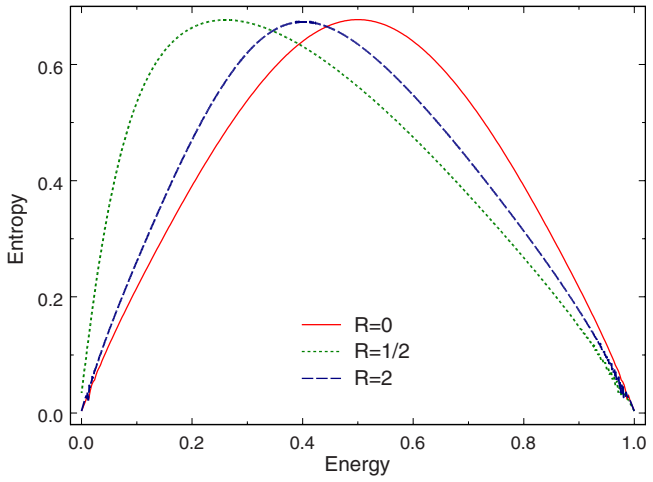

FIG. 1. (Color online) Exact entropy $s(e)=[\ln \Omega(e)]/200$ (in unit of k_B) as a function of energy e of the 10×20 square-lattice Ising model for $R=0$, $\frac{1}{2}$, and 2, where $e=E/E_{\max}=(E_1+RE_2)/E_{\max}$.

$\Omega(E_1,E_2)$ is about 26 days on a Linux PC with one Intel E6600 CPU.

For $L=10$, because of memory limitations, $\Omega(E=E_1+RE_2)$ instead of $\Omega(E_1,E_2)$ is evaluated for a fixed value of $R=J_2/J_1$. Because data for R and $-R$ values provide the same information, we consider only $R>0$ in this paper. The CPU time for the evaluation of $\Omega(E)$ on the same PC is about 11 days for $R=5$ ($E_{\max}=2000$) and about 21 days for $R=10$ ($E_{\max}=3800$). With $\Omega(E)$, the partition function is then given by

$$Z_R=\sum_{E=0}^{E_{\max}}\Omega(E)a^E, \tag{3}$$

where $a=e^{2\beta J_1}$.

Figure 1 shows the entropy $s(e)/k_B=[\ln \Omega(e)]/200$, as a function of energy $e(=E/E_{\max})$, of the 10×20 square-lattice Ising model for $R=0$, $\frac{1}{2}$, and 2. As shown in the figure, the entropy is symmetric for $R=0$ but asymmetric for $R\neq 0$. The entropy has the maximum $s_{\max}=0.6772k_B$ at $e=0.5$ for $R=0$, $s_{\max}=0.6767k_B$ at $e=0.261$ for $R=\frac{1}{2}$, and $s_{\max}=0.6733k_B$ at $e=0.401$ for $R=2$. As R varies from $R=0$ to $\frac{1}{2}$, the entropy maximum moves away from the midpoint $e=0.5$. On the other hand, as R varies from $\frac{1}{2}$ to ∞, the maximum moves back to $e=0.5$.

III. PARTITION FUNCTION ZEROS

It is well-known [20] that the partition function zeros in the complex $a=e^{2\beta J_1}$ plane of the square-lattice Ising model for $R=0$ lie on the two circles $a_1=1+\sqrt{2}e^{i\theta}$ and $a_2=-1+\sqrt{2}e^{i\theta}$ in the thermodynamic limit, as shown in Fig. 2(a). Also, the distributions of the partition function zeros determine the properties of the Ising model for $R=0$ [20]. However, the behavior and properties of the partition function zeros for $R\neq 0$ are not known.

Figure 2 shows the partition function zeros in the complex a plane of the 10×20 square-lattice Ising model for various values of R, obtained from

$$Z_R=\sum_E \Omega(E)a^E=C(R)\prod_{i=1}^{E_{\max}}[a-a_i(R)], \tag{4}$$

where $C(R)$ is a constant. As shown in the figure, there is no zero around the origin. The overall tendency in the distribution of the zeros for $R=1$ is somewhat similar to that for $R=0$. As R increases, the distribution of the zeros becomes more complex, and the size of substructure in the distribution decreases and the number of substructure increases from 4 for $R=2$ to 10 for $R=5$ and 20 for $R=10$. It seems that the number of substructure is equal to $2R$.

When R is not an integer multiple of $\frac{1}{2}$, the expression for the partition function, Eq. (3), cannot be used. Instead, the partition function is expressed as

$$Z_R=\sum_{E'=0}\Omega(E')e^{\beta J_1 E'} \tag{5}$$

for $R=\frac{N}{4}$ (N: odd numbers) and

$$Z_R=\sum_{E''=0}\Omega(E'')e^{\beta J_1 E''/2} \tag{6}$$

for $R=\frac{N}{8}$ (N: odd numbers). Figure 3 shows the partition function zeros of the 9×18 square-lattice Ising model (a) in the complex $x=a^{1/2}=e^{\beta J_1}$ plane for $R=\frac{9}{4}$ and (b) in the complex $y=a^{1/4}=e^{\beta J_1/2}$ plane for $R=\frac{9}{8}$, respectively. Again, the substructures appear in the zero distributions. The number of substructure is $4R$ for $R=\frac{N}{4}$ (N: even and odd numbers) in the complex x plane, $8R$ for $R=\frac{N}{8}$ in the complex y plane, $16R$ for $R=\frac{N}{16}$ in the complex $a^{1/8}=e^{\beta J_1/4}$ plane, and so on.

A. $R\to\infty$ case

In the limit $J_2\to\infty(R\to\infty)$, the partition function can be written as

$$Z=\sum_{E_1=0}^{N_1}\Omega(E_1,E_2=N_2)e^{2\beta(J_1E_1+J_2N_2)}. \tag{7}$$

Because the density of states $\Omega(E_1,N_2)$ has nonzero values only for $E_1=0$ and $E_1=N_1$, the partition function becomes

$$Z=2e^{2\beta J_2N_2}(1+e^{2\beta J_1N_1}). \tag{8}$$

Therefore, the partition function zeros in the complex $a=e^{2\beta J_1}$ plane are given by

$$a_n=\exp[i(2n-1)\pi/N_1], \tag{9}$$

where $n=1,\ldots,N_1$. That is, they are uniformly distributed on the unit circle. Figure 4 shows the partition function zeros in the complex a plane of the 4×8 square-lattice Ising model for $R=50$. Even though the value of $R=50$ is not too large, the zeros already lie close to the unit circle.

On the other hand, in the limit $J_1\to 0$ $(R\to\infty)$, where the model reduces to two decoupled Ising models with only next-nearest-neighbor interactions, the partition function is expressed as

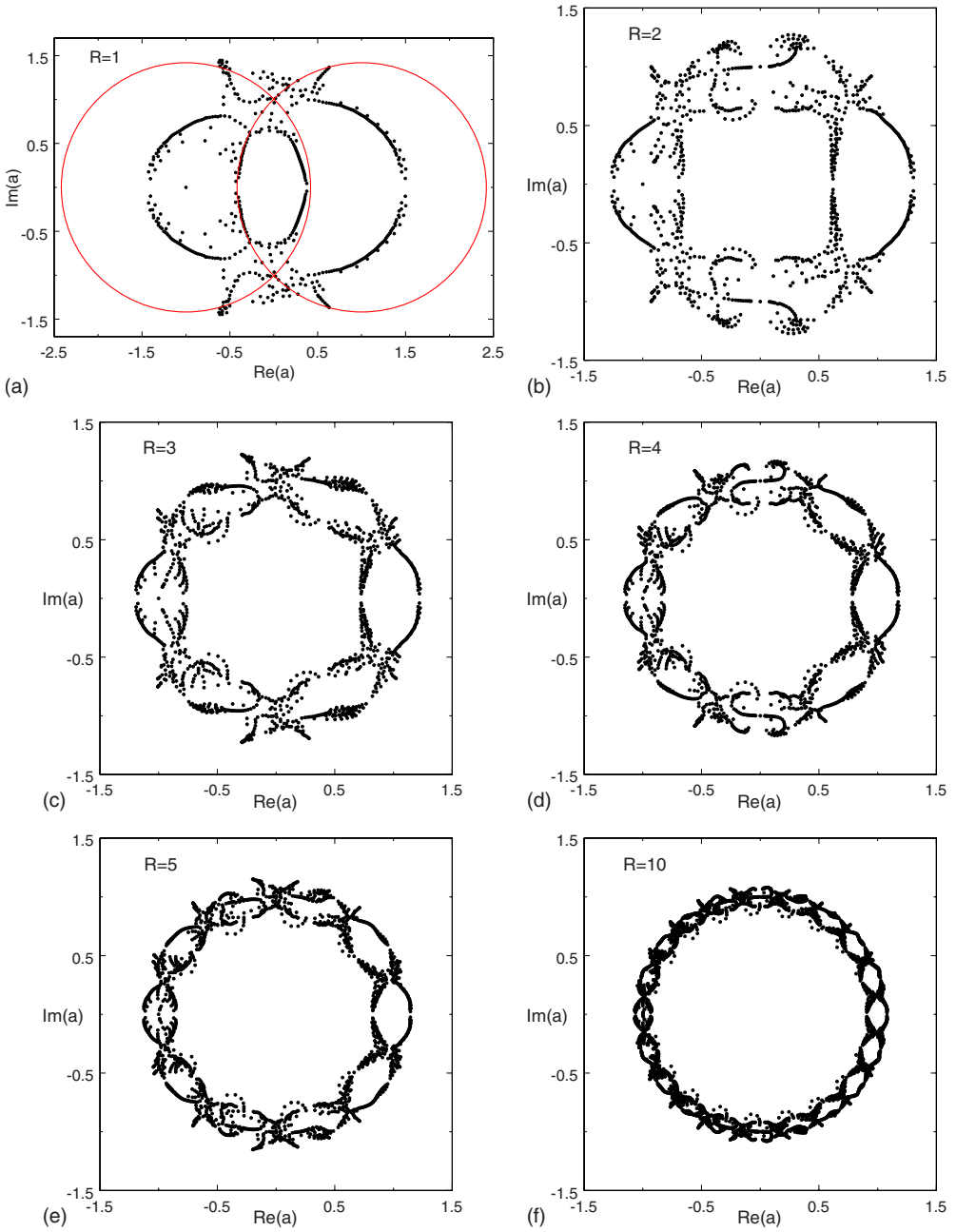

FIG. 2. (Color online) Partition function zeros in the complex $a=e^{2\beta J_1}$ plane of the 10×20 square-lattice Ising model for (a) $R=1$, (b) 2, (c) 3, (d) 4, (e) 5, and (f) 10. In (a), the loci (two circles) of the zeros for $R=0$ in the thermodynamic limit are shown for comparison. The total number of zeros is 560 for $R=1$, 920 for $R=2$, 1280 for $R=3$, 1640 for $R=4$, 2000 for $R=5$, and 3800 for $R=10$, respectively.

$$Z=\sum_{E_2=0}^{N_2}\left[\sum_{E_1=0}^{N_1}\Omega(E_1,E_2)\right]e^{2\beta J_2E_2}. \tag{10}$$

$$Z=\sum_{E_2=0}^{N_2}\tilde{\Omega}(E_2)e^{2\beta J_2E_2}=Z_0^2=\left[\sum_{E_0=0}^{N_2/2}\Omega_0(E_0)e^{2\beta J_2E_0}\right]^2. \tag{11}$$

For example, Table I shows the summation of the density of states over E_1, $\tilde{\Omega}(E_2)=\Sigma_{E_1}\Omega(E_1,E_2)$, on 4×8 square lattice. Then the partition function Z is equivalent to the square of the partition function Z_0 of the nearest-neighbor-interaction Ising model as follows:

Also, Table II shows the density of states $\Omega_0(E_0)$ of the 4×8 square-lattice Ising model for $J_1=0$ on a sublattice, which readily reproduces $\tilde{\Omega}(E_2)$ in Table I. Therefore, the partition function zeros in the complex $b=e^{2\beta J_2}$ plane lie on the well-known two circles $b_1=1+\sqrt{2}e^{i\theta}$ and $b_2=-1+\sqrt{2}e^{i\theta}$ in the thermodynamic limit.

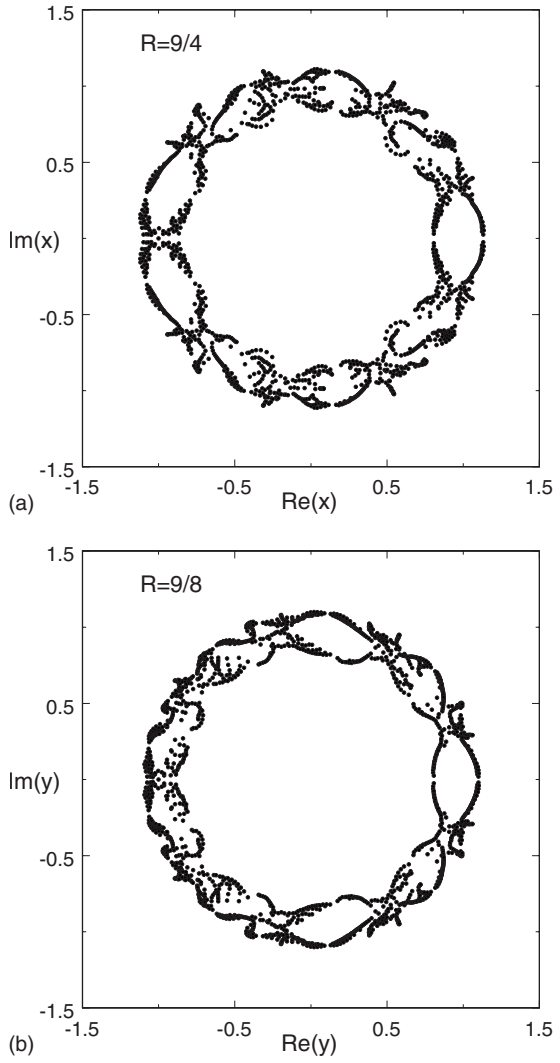

FIG. 3. Partition function zeros of the 9×18 square-lattice Ising model (a) in the complex $x=e^{\beta J_1}$ plane for $R=\frac{9}{4}$ and (b) in the complex $y=e^{\beta J_1/2}$ plane for $R=\frac{9}{8}$. The total number of zeros is 1620 for $R=\frac{9}{4}$ and 1944 for $R=\frac{9}{8}$, respectively.

B. Critical behaviors

The partition function zeros, in the case that they cross the positive real axis in the thermodynamic limit, determine the critical points and exponents. As shown in Fig. 2, there are two branches of the zeros near the positive real axis. The zeros near the positive real axis for $a<1$ (that is, $J_1<0$ and consequently $J_2<0$) determine the antiferromagnetic ($0\le R<\frac{1}{2}$) or superantiferromagnetic ($R>\frac{1}{2}$) critical points, while the zeros for $a>1$ ($J_1>0$ and $J_2>0$) do the ferromagnetic critical points ($R\ge0$).

As a test, extrapolating the finite-size data for $L=4\sim10$ with Bulirsch-Stoer (BST) method [24,25], we have estimated the critical points and exponents for $R=0$, where the ferromagnetic and antiferromagnetic critical points are known to be $a_c^{\rm fm}=1+\sqrt{2}=2.41421356$ and $a_c^{\rm af}=-1+\sqrt{2}=0.41421356$ and the thermal scaling exponent to be $y_t=1/\nu=1$ for both cases. For finite lattices, we evaluate the thermal scaling exponent [15,23]

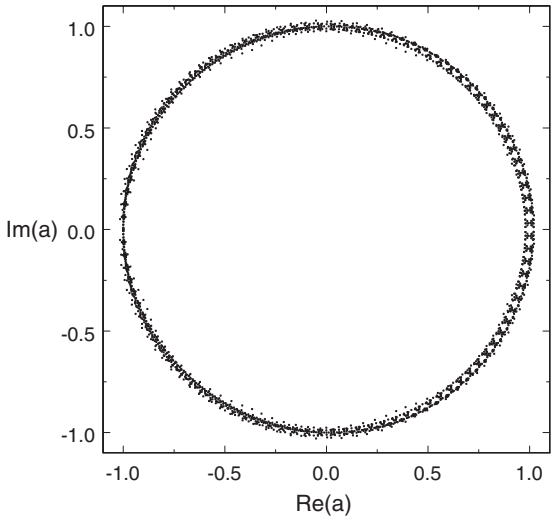

FIG. 4. Partition function zeros in the complex a plane of the 4×8 square-lattice Ising model for $R=50$. The total number of zeros is 2432.

$$y_t(L)=-\frac{\ln\{\mathrm{Im}[a_1(L+1)]/\mathrm{Im}[a_1(L)]\}}{\ln[(L+1)/L]}, \tag{12}$$

following the finite-size scaling $\mathrm{Im}[a_1(L)]\sim L^{-y_t}$ for the imaginary part $\mathrm{Im}[a_1(L)]$ of the first zero $a_1(L)$ that is the closest zero to the positive real axis. We have obtained $a_c^{\rm fm}=2.414217(5)+0.0000(64)i$ and $y_t^{\rm fm}=1.00003(6)$ and $a_c^{\rm af}=0.4142135(4)+0.000000(7)i$ and $y_t^{\rm af}=0.9999(1)$, using the parameter $\omega=1$ of the BST algorithm. The error estimates are twice the difference between the $(n-1,1)$ and $(n-1,2)$ approximants. Our results are in excellent agreement with the exact values.

Table III shows the estimated values of the critical points a_c (zero) and the thermal scaling exponent y_t for the square-lattice Ising ferromagnet and antiferromagnet. The values of the thermal scaling exponents for $R\neq0$ are consistent with the exact result $y_t=1$ for $R=0$, indicating the universal critical behavior with varying R. The values, a_c (Zandvliet), of Zandvliet formula (closed-form approximation) [14] for the ferromagnetic and antiferromagnetic critical points are also shown in the table. Our results and Zandvliet values agree for small values of R (for example, differences of 0.2% for $R=\frac{1}{4}$ (FM) and 0.5% for $R=\frac{1}{2}$), but the differences between two values are not negligible (about or over 1% difference) for most values of R.

Table IV shows the estimated values of the critical points and thermal scaling exponent for the square-lattice Ising superantiferromagnet. In addition, the values of Berker-Hui formula (closed-form approximation) [11] and Swendsen-Krinsky formula (phenomenological parametric approximation to the fourth order in J_1/J_2) [3] for the critical points are shown in the table for comparison. Our results and Berker-Hui values are close each other, showing the largest difference between two values for $R=1$ (0.3%) and the smallest difference for $R=4$ (0.002%). Within errors, Swendsen-Krinsky values are in agreement with our results for $R=1$, 2, 3, and 10 (differences of 0.09% for $R=1$, 0.005% for $R=2$,

TABLE I. The summation of the density of states over E_1, $\tilde{\Omega}(E_2)=\Sigma_{E_1}\Omega(E_1,E_2)$, for the 4×8 square-lattice Ising model.

E_2	$\tilde{\Omega}$ (E_2)	E_2	$\tilde{\Omega}$ (E_2)	E_2	$\tilde{\Omega}$ (E_2)
0 and 48	4	2 and 46	64	4 and 44	736
6 and 42	8640	8 and 40	73848	10 and 38	516032
12 and 36	3270112	14 and 34	16987712	16 and 32	69378556
18 and 30	214714752	20 and 28	496374592	22 and 26	841252480
24	1009812240				

0.004% for $R=3$, and 0.006% for $R=10$, respectively). Our results and Swendsen-Krinsky values are very close for $R=4$ and 5, but show little differences due to small error values (differences of 0.01% for $R=4$ and 0.03% for $R=5$). More importantly, the values of the thermal scaling exponents are clearly different from $y_t=1$, and they decreases (nonuniversal critical behavior) as R increases. For $R=1$ and 2, the comparison between the current results of y_t and those of other works has been reported in Ref. [15]. For $R>2$, there is no published result of y_t to directly compare with ours.

Barber studied the square-lattice Ising superantiferromagnet near $J_1=0$ ($R=\infty$) by perturbation theory [4]. He obtained the formulas for the critical point and specific-heat critical exponent to the second order in J_1/J_2. Barber formulas yield the values of $a_c=0.915390$ and $y_t=1.0075$ for $R=10$. The Barber value of the critical point is comparable to those in Table IV, and the value of the thermal scaling exponent is slightly different from our result of $y_t=1.0151(5)$.

C. $R=\frac{1}{2}$ case

The case $R=\frac{1}{2}$ ($J_1<0$ and $J_2<0$) is special in that the antiferromagnetic and superantiferromagnetic ordered states have the same energy, that is, $R=\frac{1}{2}$ is the frontier between the antiferromagnetic ($R<\frac{1}{2}$) and superantiferromagnetic ($R>\frac{1}{2}$) phases. It is believed that there is no phase transition at finite temperatures due to the ground-state degeneracy for $R=\frac{1}{2}$ [1,5,6,9,12,17,18].

Figure 5 shows the partition function zeros in the complex a plane of the 10×20 square-lattice Ising model for $R=\frac{1}{2}$. The most prominent feature in the distribution of the zeros for $R=\frac{1}{2}$ is that some zeros lie close to the origin (corresponding to zero temperature), as shown in the figure. Again extrapolating the finite-size data for $L=4\sim 10$ with the BST algorithm, we have obtained $a=0.0025(7)+0.00000(2)i$ and $y_t=1.94(7)$, implying the possibility of $y_t=2$. For $R=\frac{1}{2}$, Berker-Hui formula gives no information, while Zandvliet formula and Swendsen-Krinsky formula yield $a_Z=0$ and $a_{SK}=0.061(5)$, respectively.

If we assume that the zeros cross the origin in the thermodynamic limit, we have

$$a=e^{2\beta J_1}\sim \xi^{-y_t}, \tag{13}$$

where ξ is the correlation length. Furthermore, if we accept the value of $y_t=2$, the correlation length behaves such as

$$\xi\sim e^{-\beta J_1}=e^{-J_1/(k_BT)}, \tag{14}$$

indicating its exponential divergence ($J_1<0$) at $T=0$. Based on the assumption that the correlation length has the exponential divergence at $T=0$ for $R=\frac{1}{2}$,

$$\xi\sim \exp[cT^{-\bar{\nu}}], \tag{15}$$

Landau obtained the numerical result of $\bar{\nu}\approx 1$ [5]. Landau's result is the same as Eq. (14). Also, the value of $y_t=2$ may be interpreted in two dimensions ($d=2$) as an indication of the first-order phase transition at $T=0$, according to the Fisher-Berker scaling theory for first-order phase transition ($y_t=d$) [26].

IV. CONCLUSION

For the Ising model with nearest-neighbor (J_1) and next-nearest-neighbor (J_2) interactions, the exact integer values for the density of states $\Omega(E_1,E_2)$ have been evaluated on $L\times 2L$ (up to $L=9$) square lattices using the microcanonical transfer matrix, and for $L=10$ $\Omega(E=E_1+RE_2)$ has been calculated up to $R=J_2/J_1=10$. Using the density of states, the distributions of the partition function zeros have been ob-

TABLE II. The density of states $\Omega_0(E_0)$ of the 4×8 square-lattice Ising model for $J_1=0$ on a sublattice.

E_0	Ω_0 (E_0)	E_0	Ω_0 (E_0)	E_0	Ω_0 (E_0)
0 and 24	2	2 and 22	16	4 and 20	120
6 and 18	1200	8 and 16	5262	10 and 14	14912
12	22512				

TABLE III. The values of the critical points, a_c (zero), and the thermal scaling exponent, $y_t(R)$, for the square-lattice Ising ferromagnet ($R=\frac{1}{4}$ (FM), $\frac{1}{2}$, 1,..., and 10) and the antiferromagnet [$R=\frac{1}{4}$ (AF)], estimated using the partition function zeros ($L=4\sim10$). In the BST extrapolation, the parameter $\omega=1$ is used. In addition, the values of Zandvliet formula for the critical points, a_c (Zandvliet), are shown for comparison.

R	a_c (Zandvliet)	a_c (zero)	y_t (R)
$\frac{1}{4}$ (AF)	0.25	0.2480(1)	1.003(3)
$\frac{1}{4}$ (FM)	1.922302	1.92591(1)	1.0001(2)
$\frac{1}{2}$	1.683772	1.69150(3)	1.0001(5)
1	1.450405	1.46282(4)	1.0012(7)
2	1.267561	1.28249(5)	1.002(1)
3	1.190278	1.20505(3)	1.0041(4)
4	1.147629	1.16162(2)	1.004(2)
5	1.120596	1.13377(4)	1.005(1)
10	1.062953	1.07261(2)	0.996(4)

tained in the complex $a=e^{2\beta J_1}$ plane. The partition function zeros lie on the well-known two circles $a=\pm1+\sqrt{2}e^{i\theta}$ for $R=0$, whereas they lie on the unit circle $a=e^{i\theta}$ for $R=\infty$. Between these two ends, as R increases, the number of substructure in the distribution of the zeros increases, and the size of substructure decreases.

Using the partition function zeros, the critical point $a_c(R)$ and the thermal scaling exponent $y_t(R)$ have been estimated for the Ising ferromagnet, antiferromagnet, and superantiferromagnet. Our results have been compared with those of Zandvliet formula for the ferromagnetic critical point and of Berker-Hui formula and Swendsen-Krinsky formula for the superantiferromagnetic critical point. For $R=10$, our results of the superantiferromagnet have also been compared to those by perturbation theory.

For the special case of $R=\frac{1}{2}$ ($J_1<0$ and $J_2<0$), where the antiferromagnetic and superantiferromagnetic ordered states have the same energy, the results based on the partition function zeros may be interpreted as the exponential divergence of the correlation length at zero temperature.

TABLE IV. The values of the critical points, a_c (zero), and the thermal scaling exponent, $y_t(R)$, for the square-lattice Ising superantiferromagnet, estimated using the partition function zeros ($L=4\sim10$). In the BST extrapolation, we have used the parameter $\omega=1$ for the estimation of $y_t(R)$ and the parameter $\omega=y_t(R)$ for the estimation of a_c (zero). Also, the values of Berker-Hui formula a_c (BH) and Swendsen-Krinsky formula a_c (SK) for the critical points are shown for comparison.

R	a_c (BH)	a_c (SK)	a_c (zero)	y_t (R)
1	0.381966	0.3827(15)	0.3830(2)	1.181(1)
2	0.637882	0.6383(2)	0.6382(7)	1.066(1)
3	0.743507	0.74366(6)	0.74363(2)	1.050(1)
4	0.801375	0.80145(3)	0.80136(2)	1.042(1)
5	0.837924	0.837965(14)	0.83775(4)	1.036(1)
10	0.915572	0.915578(2)	0.91552(44)	1.0151(5)

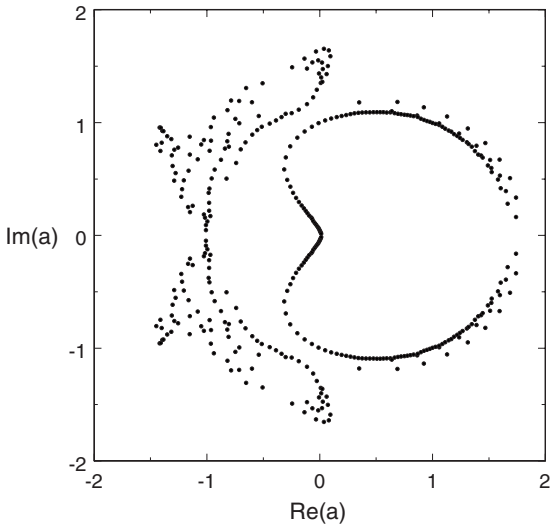

FIG. 5. Partition function zeros in the complex a plane of the 10×20 square-lattice Ising model for $R=\frac{1}{2}$.

ACKNOWLEDGMENTS

This work was supported by the Korea Research Foundation Grant funded by the Korean Government (Grant No. KRF-2008-313-C00332).

APPENDIX: MICROCANONICAL TRANSFER MATRIX

In this appendix, the microcanonical transfer matrix is briefly described for $L=4$ on $L\times2L$ square lattice with free boundary conditions in the L direction and periodic boundary conditions in the $2L$ direction. First, an array $\omega^{(2)}$, which is indexed by E_1, E_2, and spin variables $\sigma_i^{(1)}$ and $\sigma_i^{(2)}$ ($1\le i\le4$) for the first and second rows, is initialized as

$$\begin{aligned}\omega^{(2)}(E_1,E_2,\{\sigma_i^{(1)}\},\{\sigma_i^{(2)}\}) &= \delta\left(E_1-\frac{1}{2}\sum_{n=1}^{3}[\sigma_n^{(1)}\sigma_{n+1}^{(1)}+\sigma_n^{(2)}\sigma_{n+1}^{(2)}+2]\right.\\ &\quad\left.-\frac{1}{2}\sum_{n=1}^{4}[\sigma_n^{(1)}\sigma_n^{(2)}+1]\right)\\ &\quad\times\delta\left(E_2-\frac{1}{2}\sum_{n=1}^{3}[\sigma_n^{(1)}\sigma_{n+1}^{(2)}+\sigma_{n+1}^{(1)}\sigma_n^{(2)}+2]\right).\end{aligned} \tag{A1}$$

Next, by introducing spin variables $\sigma_i^{(3)}$ ($1\le i\le4$) for the third row and considering the vertical and diagonal bonds between the second and third rows, the array $\omega^{(2)}$ is modified into

$$\tilde{\omega}^{(3)}(E_1,E_2,\{\sigma_i^{(1)}\},\{\sigma_i^{(3)}\}) = \sum_{\{\sigma_i^{(2)}\}} \omega^{(2)}\left(E_1 - \frac{1}{2}\sum_{n=1}^{4}[\sigma_n^{(2)}\sigma_n^{(3)}+1], E_2 - \frac{1}{2}\sum_{n=1}^{3}[\sigma_n^{(2)}\sigma_{n+1}^{(3)} + \sigma_{n+1}^{(2)}\sigma_n^{(3)} + 2], \{\sigma_i^{(1)}\}, \{\sigma_i^{(2)}\}\right). \quad \text{(A2)}$$

Then, the horizontal bonds connecting the spins in the third row are taken into account by shifting the energy:

$$\omega^{(3)}(E_1,E_2,\{\sigma_i^{(1)}\},\{\sigma_i^{(3)}\}) = \tilde{\omega}^{(3)}\left(E_1 - \frac{1}{2}\sum_{n=1}^{3}[\sigma_n^{(3)}\sigma_{n+1}^{(3)}+1], E_2, \{\sigma_i^{(1)}\}, \{\sigma_i^{(3)}\}\right). \quad \text{(A3)}$$

These two procedures, Eqs. (A2) and (A3), are then applied to each row in turn until the final (eighth) row is reached, where we have

$$\omega^{(8)}(E_1,E_2,\{\sigma_i^{(1)}\},\{\sigma_i^{(8)}\}). \quad \text{(A4)}$$

Finally, the vertical and diagonal bonds between the first and eighth rows are then taken into account by the following equation:

$$\tilde{\Omega}(E_1,E_2,\{\sigma_i^{(1)}\}) = \sum_{\{\sigma_i^{(8)}\}} \omega^{(8)}\left(E_1 - \frac{1}{2}\sum_{n=1}^{4}[\sigma_n^{(8)}\sigma_n^{(1)}+1], E_2 - \frac{1}{2}\sum_{n=1}^{3}[\sigma_n^{(8)}\sigma_{n+1}^{(1)} + \sigma_{n+1}^{(8)}\sigma_n^{(1)} + 2], \{\sigma_i^{(1)}\}, \{\sigma_i^{(8)}\}\right). \quad \text{(A5)}$$

The density of states is then given by

$$\Omega(E_1,E_2) = \sum_{\{\sigma_i^{(1)}\}} \tilde{\Omega}(E_1,E_2,\{\sigma_i^{(1)}\}). \quad \text{(A6)}$$

[1] M. Nauenberg and B. Nienhuis, Phys. Rev. Lett. **33**, 944 (1974).
[2] M. P. Nightingale, Phys. Lett. A **59**, 486 (1977).
[3] R. H. Swendsen and S. Krinsky, Phys. Rev. Lett. **43**, 177 (1979).
[4] M. N. Barber, J. Phys. A **12**, 679 (1979).
[5] D. P. Landau, Phys. Rev. B **21**, 1285 (1980).
[6] J. Oitmaa, J. Phys. A **14**, 1159 (1981).
[7] D. P. Landau and K. Binder, Phys. Rev. B **31**, 5946 (1985).
[8] H. W. J. Blote, A. Compagner, and A. Hoogland, Physica A **141**, 375 (1987).
[9] M. D. Grynberg and B. Tanatar, Phys. Rev. B **45**, 2876 (1992).
[10] K. Minami and M. Suzuki, Physica A **195**, 457 (1993).
[11] A. N. Berker and K. Hui, Phys. Rev. B **48**, 12393 (1993).
[12] J. L. Moran-Lopez, F. Aguilera-Granja, and J. M. Sanchez, J. Phys.: Condens. Matter **6**, 9759 (1994).
[13] A. Malakis, P. Kalozoumis, and N. Tyraskis, Eur. Phys. J. B **50**, 63 (2006).
[14] H. J. W. Zandvliet, Europhys. Lett. **73**, 747 (2006).
[15] J. L. Monroe and S.-Y. Kim, Phys. Rev. E **76**, 021123 (2007).
[16] A. Nußbaumer, E. Bittner, and W. Janke, EPL **78**, 16004 (2007).
[17] A. Kalz, A. Honecker, S. Fuchs, and T. Pruschke, Eur. Phys. J. B **65**, 533 (2008).
[18] R. A. dos Anjos, J. R. Viana, and J. R. de Sousa, Phys. Lett. A **372**, 1180 (2008).
[19] C. N. Yang and T. D. Lee, Phys. Rev. **87**, 404 (1952); **87**, 410 (1952).
[20] M. E. Fisher, in *Lectures in Theoretical Physics*, edited by W. E. Brittin, (University of Colorado Press, Boulder, CO, 1965), Vol. 7c, p. 1.
[21] I. Bena, M. Droz, and A. Lipowski, Int. J. Mod. Phys. B **19**, 4269 (2005) and references therein.
[22] H. Stamerjohanns, O. Mulken, and P. Borrmann, Phys. Rev. Lett. **88**, 053401 (2002); R. A. Blythe and M. R. Evans, *ibid.* **89**, 080601 (2002); N. A. Alves and U. H. E. Hansmann, J. Chem. Phys. **117**, 2337 (2002); Y. Peng, U. H. E. Hansmann, and N. A. Alves, *ibid.* **118**, 2374 (2003); J. Wang and W. Wang, *ibid.* **118**, 2952 (2003); Y. Kafri and D. Mukamel, Phys. Rev. Lett. **91**, 055502 (2003); I. Bena, F. Coppex, M. Droz, and A. Lipowski, *ibid.* **91**, 160602 (2003); S.-Y. Kim, *ibid.* **93**, 130604 (2004); N. Bastid, FOPI Collaboration *et al.*, Phys. Rev. C **72**, 011901 (2005); R. Kenna, D. A. Johnston, and W. Janke, Phys. Rev. Lett. **96**, 115701 (2006); P. Tong and X. Liu, *ibid.* **97**, 017201 (2006); P. Y. Chan, N. Goldenfeld, and M. Salamon, *ibid.* **97**, 137201 (2006); R. Kenna, D. A. Johnston, and W. Janke, *ibid.* **97**, 155702 (2006); P. Cejnar, S. Heinze, and M. Macek, *ibid.* **99**, 100601 (2007); B. I. Abelev, STAR Collaboration *et al.*, Phys. Rev. C **77**, 054901 (2008); N. Yamamoto and T. Kanazawa, Phys. Rev. Lett. **103**, 032001 (2009) and references therein.
[23] R. J. Creswick, Phys. Rev. E **52**, R5735 (1995).
[24] J. L. Monroe, Phys. Rev. E **65**, 066116 (2002).
[25] R. Bulirsch and J. Stoer, Numer. Math. **6**, 413 (1964); M. Henkel and A. Patkos, J. Phys. A **20**, 2199 (1987).
[26] M. E. Fisher and A. N. Berker, Phys. Rev. B **26**, 2507 (1982).